Exploring the impact of inoculum dose on host immunity and morbidity to inform model-based vaccine design

2018-04-30

Authors

- Andreas Handel[1], Department of Epidemiology and Biostatistics, The University of Georgia, Athens, GA, USA
- Yan Li, Institute of Bioinformatics, The University of Georgia, Athens, GA, USA. Current address: Center for Research Informatics, University of Chicago, Chicago, IL, USA
- Brian McKay, Department of Epidemiology and Biostatistics, The University of Georgia, Athens, GA, USA
- Kasia A. Pawelek, Department of Mathematics and Computational Science, University of South Carolina Beaufort, Bluffton, SC, USA
- Veronika Zarnitsyna, Department of Microbiology and Immunology, Emory University School of Medicine, Atlanta, GA, USA
- Rustom Antia, Department of Biology, Emory University, Atlanta, GA, USA

[1] corresponding author: ahandel@uga.edu

Abstract

Background: Vaccination is an effective method to protect against infectious diseases. An important consideration in any vaccine formulation is the inoculum dose, i.e., amount of antigen or live attenuated pathogen that is used. Higher levels generally lead to better stimulation of the immune response but might cause more severe side effects and allow for less population coverage in the presence of vaccine shortages. Determining the optimal amount of inoculum dose is an important component of rational vaccine design. A combination of mathematical models with experimental data can help determine the impact of the inoculum dose.

Methods: We designed mathematical models and fit them to data from influenza A virus (IAV) infection of mice and human parainfluenza virus (HPIV) of cotton rats at different inoculum doses. We used the model to predict the level of immune protection and morbidity for different inoculum doses and to explore what an optimal inoculum dose might be.

Results: We show how a framework that combines mathematical models with experimental data can be used to study the impact of inoculum dose on important outcomes such as immune protection and morbidity. We find that the impact of inoculum dose on immune protection and morbidity depends on the pathogen and both protection

and morbidity do not always increase with increasing inoculum dose. An intermediate inoculum dose can provide the best balance between immune protection and morbidity, though this depends on the specific weighting of protection and morbidity.

Conclusions: Once vaccine design goals are specified with required levels of protection and acceptable levels of morbidity, our proposed framework which combines data and models can help in the rational design of vaccines and determination of the optimal amount of inoculum.

Introduction

Vaccines are the best and most cost-effective defenses we have against many infectious diseases. While the composition of a vaccine can be complex, the most important component is the antigen of the pathogen against which one wants to immunize [1]. Different types of vaccines exist, those based on antigens that contain the pathogen in a non-replicating form, and those that contain the pathogen in a replicating form, usually attenuated to reduce morbidity and mortality [1].

When deciding on the inoculum dose for a vaccine, one often needs to strike a balance between conflicting goals. Higher doses generally lead to more immunity and better protection [2]. Lower doses might reduce vaccine side effects and might also be required if there is a vaccine shortage, for instance due to a pandemic emergency, manufacturing issues or high costs [3,4]. The ability to predict how changes in inoculum dose impact immune protection and morbidity, and how to achieve the best balance between enough inoculum to trigger a robust immune response and low enough inoculum would significantly contribute toward better vaccine design [5–12].

Currently, the main way to determine vaccine inoculum dose is by trial and error, which is expensive and logistically challenging [13–16]. A way to improve this approach is to combine mathematical models with experimental data. Such approaches are commonly applied to drugs, where pharmacokinetic/pharmacodynamic (PK/PD) models are used in combination with experimental data to try and optimize drug dosing regimens [17]. Application of a similar approach to vaccines has been recently proposed for tuberculosis [18].

Here, we develop and analyze a quantitative modeling framework that might allow us to eventually predict the optimal inoculum dose for a given vaccine and setting. We develop our modeling framework for live attenuated vaccines using data from two infection experiments, namely influenza A virus (IAV) and human parainfluenza virus (HPIV). We further investigate a scenario for an inactivated vaccine.

Influenza A virus remains a serious health concern. While a vaccine exists, it needs to be reformulated regularly. Even when the vaccine is well-matched to the circulating strain, its efficacy is not as good as that of other vaccines, especially in the elderly. It has been suggested that using a higher inoculum dose in vaccines for this population might be beneficial [19]. Development of a better vaccine that remains protective in the presence of antigenic drift and that has a higher efficacy remains a priority.

Human parainfluenza virus (HPIV) is an important cause of lower respiratory tract illness in children [20–24]. There is currently no licensed vaccine available against HPIV [11,21,24], despite various attempts to develop such a vaccine [25].

While the two pathogens we analyze here are important on their own, we consider the most important contribution of this study to be the development of a conceptual, quantitative framework that may be used to rationally design vaccines and determine an optimal inoculum dose for any pathogen.

Materials and Methods

Experimental data

We analyzed data from two previously published studies, one on influenza A virus (IAV) infections in mice [26] and the other on human parainfluenza virus (HPIV) type 3 infection in cotton rats [27].

For the IAV study, groups of mice were infected with 6 different inoculum doses of the H1N1 PR8 strain of influenza. Geometric mean viral titers were recorded at different times following the infection with each dose. In addition, lung damage was measured and scored.

For the HPIV study, groups of cotton rats were infected with 5 different doses of HPIV-3. Geometric mean viral titers were recorded at different times following infection in both lung and nose. For the highest inoculum dose, the study additionally reported several virus measurements over the first 96 hours. The study also reported antibody titers 21 days after infection for the 3 lowest inoculum doses for which virus data was reported.

We used an additional data set to estimate a mapping between innate immune response strength and morbidity. This data was taken from a previously reported challenge study of influenza infection in human volunteers [28]. We used the reported values for different components of the innate response (IFN-a, IL6, IL8 and TNF-a) and total symptom score as measure of morbidity.

For further experimental details, we refer the reader to the original studies.

Mechanistic dynamical infection model

We formulated and implemented a mechanistic, dynamical model of the infection dynamics based on a set of ordinary differential equations. The model is based on our previous work, where we analyzed the relationship between inoculum dose and viral load dynamics [29]. The model is also similar to many other models that have recently been used to model acute viral infections (see e.g. [30–33]).

Our model tracks target cells, virus, and certain immune response components. Uninfected cells, U, become infected by free virus, V, at rate b. Infected cells, I, produce virus at rate p and die at rate d_I. For purposes of comparison with the data, we keep track of dead cells through an extra compartment, D.

Free virus infects cells at rate b', is cleared by antibodies at rate k'_A or removed due to other mechanisms (e.g. mechanical transport) at rate d_V. Note that b' and k'_A differ from parameters b and k_A to account for experimental units (PFU for virus and titer for antibody). Since we are modeling short, acute infections, we follow the usual assumption and ignore growth and death of uninfected target cells [30,31].

In addition to the basic infection process, we also model components of the innate and adaptive immune response. We consider a generic innate response, F, which is produced and decays at rates p_F and d_F in the absence of an infection. Presence of virus leads to an increase in the innate response, with growth saturating at a maximum rate g_F. The maximum level the innate response can reach is given by the saturation parameter $F_{\max}$. Since the innate response units are arbitrary, the model is set up such that in the absence of infection, the innate response is at a steady level of $F = 1$, which leads to $p_F = d_F$. We also fix the parameter representing the decay rate at $d_F = 1$ per day, which is in line with estimates from an influenza infection analysis in ponies [34].

The innate response is modeled as having two main mechanisms of action. First, it can directly counteract the virus by, for instance, reducing virus production rate of infected cells [35]. In our model, the strength of production suppression is determined by the parameter s_F. The second action of the innate response is to induce the adaptive response, as described next.

For the adaptive response, we focus on B-cells and antibodies, which are the major correlates of protective immunity for most vaccines, including HPIV and IAV [23,36]. The dynamics of activated B cells is modeled as increasing in a sigmoidal manner dependent on both the amount of virus (antigen) and the innate response, with a maximum rate g_B. Since we are focusing on the short-term dynamics of the system, B-cell decay is ignored. In the absence of an infection, B-cells are set to an arbitrary level of 1. B-cells produce antibodies at rate r_A. Antibodies decay naturally at rate d_A and bind to and remove free virus at rate k_A.

The model is implemented as a set of ordinary differential equations given by the following set of equations:

$$\begin{aligned}
\text{Uninfected cells} \quad \dot{U} &= -bUV \\
\text{Infected cells} \quad \dot{I} &= bUV - d_I I \\
\text{Dead cells} \quad \dot{D} &= d_I I \\
\text{Virus} \quad \dot{V} &= \frac{p}{1 + s_F F} I - d_V V - k'_A A V - b' U V \\
\text{Innate response} \quad \dot{F} &= p_F - d_F F + \frac{V}{V + h_V} g_F (F_{max} - F) \\
\text{B cells} \quad \dot{B} &= \frac{F V}{F V + h_F} g_B B \\
\text{Antibodies} \quad \dot{A} &= r_A B - d_A A - k_A A V
\end{aligned} \tag{1}$$

Model fitting

The model is fit to the IAV and HPIV data. For IAV the fit is to the virus load and lung damage data. For HPIV, the fit is to the virus load and antibody data. For each pathogen, we fit data for all different inoculum doses simultaneously to the model. For each inoculum dose, i, we estimate the starting value for the virus inoculum, V_i. All other model parameters are shared across different inoculum doses.

Model performance is assessed by the sum of squared residuals (SSR). To allow computation of a single SSR value for the different experimental variables, the contribution of each variable is non-dimensionalized by dividing by the variance of the data. To give the different experimental variables comparable importance, we also divide each variable by the number of data points. This amounts to over-weighting the few data points for lung damage (AIV) and antibody response (HPIV) and reducing the weight for the more plentiful viral load data. Mathematically, the expression for the SSR is given by

$$SSR = \sum_{i,t} \frac{1}{N_{V^d}} \frac{(V_{i,t}^m - V_{i,t}^d)^2}{\sigma^2(V^d)} + \frac{1}{N_{X^d}} \frac{(X_{i,t}^m - X_{i,t}^d)^2}{\sigma^2(X^d)}$$

Here, V is viral load (on a log scale) and X represents either antibodies (for HPIV) or damage (for IAV), the superscript indicates model (m) or data (d), the sum runs over all inoculum doses, i, and all time points, t. N indicates the number of data points for either the virus or the other variable, σ^2 indicates the variance for that variable. Since both damage and antibodies (X) are measured in different units in the data and the model, each are normalized before subtracting and squaring. While this re-scaling is only necessary for the instances where we compare model and date (lung damage for IAV and antibodies for HPIV), for consistency between models, we show re-scaled values for both lung damage and antibodies for both AIV and HPIV.

The model is being fit by varying model parameters to minimize the SSR. When doing so, we take into account left-censored nature of the data. If the reported virus load is at or below the limit of detection (LOD, which is 0.27 log10 units for IAV and 2 log10 units for HPIV as reported in the original studies), we treat the difference between model and data as being the difference between model and LOD if the model prediction is above the data, and we do not count any difference between model and data for any model prediction below the LOD data point [37,38].

Model implementation

All computations were done in the R programming language version 3.4.3 [39]. Fitting was done using the nloptr optimizer package [40], differential equations were integrated using the deSolve package [41]. All data and code required to reproduce all results presented here are supplied as supplementary material.

Results

Data extraction

The data used for our study was obtained from the original reports as follows.

For the IAV study, we obtained log viral load and lung lesion score expressed in percent lung damage from table 1 of [26]. The viral kinetics of the highest inoculum dose strongly hints at survivor bias (see figure 1 of [26]). Specifically, the data suggest that sicker mice, with presumably higher virus load, were killed and sampled first, while less sick mice, with presumably lower virus load, were kept alive and sampled later. We, therefore, decided to exclude the data for the highest inoculum dose from consideration, leaving us with viral load and percent lung damage data for 5 different inoculum doses.

For the HPIV study, we focused on lung viral load. The data was extracted from figures 1 and 2 of [27] using Engauge Digitizer [42]. Viral load kinetics for the highest inoculum were measured twice with some overlap in times (24h and 96h). We averaged data for these times from the 2 experiments. We additionally obtained data on antibody titers for those inoculum doses for which viral load was reported (the 3 lowest inoculum doses) from figure 3 of [27].

For the data linking innate response to symptoms, total symptoms score data was extracted from figure 3 and innate immune response data from figures 5 and 6 of [28] using Engauge Digitizer. More details on how this data was used are provided in a later section.

Data extracted from these 3 studies are shown in Figures 1, 2 and 4 (together with the best fit models, described below), and are also included in the supplementary material.

Model development and fitting

The model we developed is described in detail in the methods section. For each data set, we fit the model to the viral load data, and either lung damage (IAV) or antibody (HPIV) data. Details on the fitting approach are provided in the methods section. The model fits and data for IAV and HPIV are shown in figures 1 and 2 respectively. Parameter values for the best fits are given in the supplementary material.

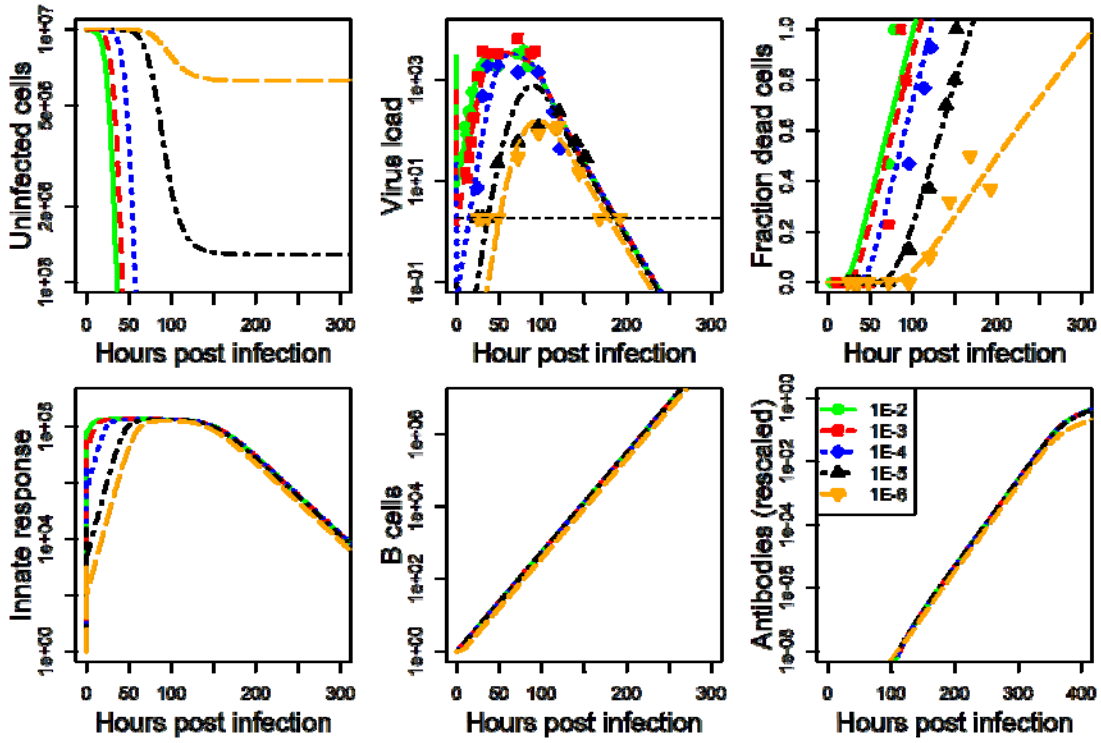

Figure 1 IAV infection at five different inoculum doses. Data was available for virus load and cell damage. Kinetics for 6 of the seven model compartments for the best fit model are shown. Infected cells kinetics very closely follows virus kinetics and is therefore not shown. Dashed horizontal line indicates the limit of detection for virus load.

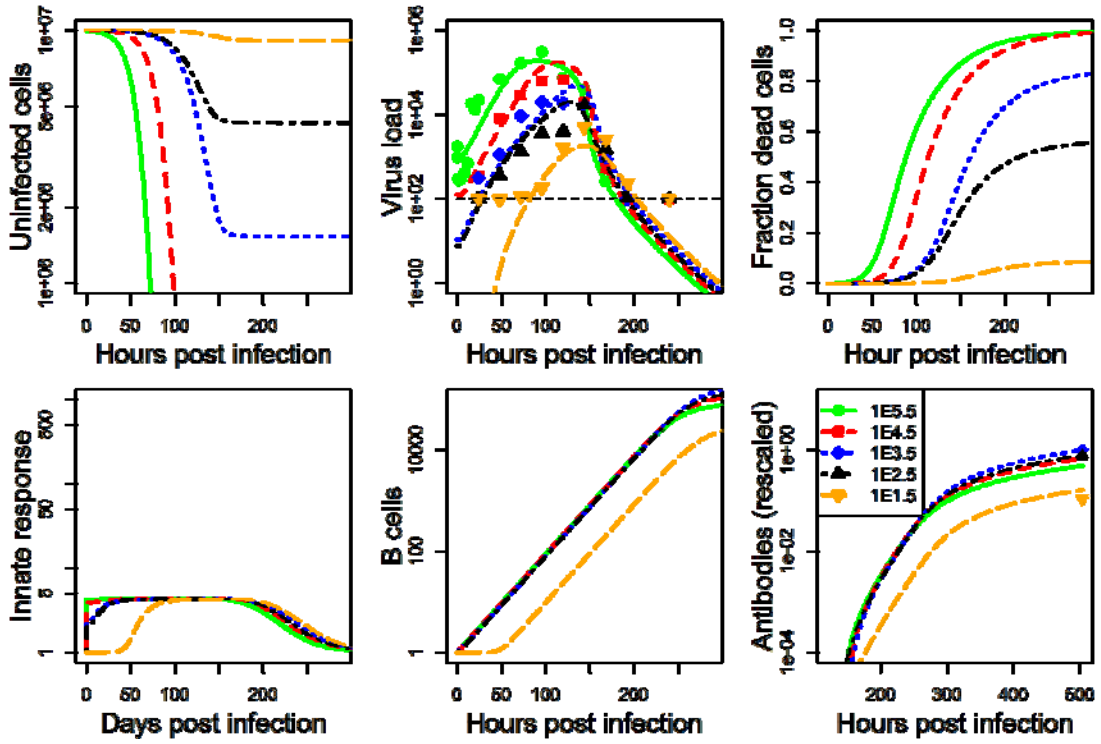

Figure 2 HPIV infection at five different inoculum doses. Data was available for virus load and antibody titers. Kinetics for 6 of the seven model compartments for the best fit model are shown. Infected cells kinetics very closely follow virus kinetics and is therefore not shown. Dashed horizontal line indicates the limit of detection for virus load.

Quantifying Immune Protection

We want to quantify the amount of protective immunity induced by different inoculum doses. We focus on the B-cell and antibody component of the adaptive immune response. Provided antibodies are specific to the pathogen, higher levels of antibodies generally lead to better protection [43–45]. Recent studies for influenza vaccines [46,47] have shown that the following function provides a good mapping from antibody titer to the level of protection from infection:

Here, the level of protection, , varies between 0 and 1, with low protection for low levels of antibody titer, , and maximum protection at high levels. The constants and determine the slope of the curve and the level at which protection is at 50% respectively (see [46] for more details). This functional shape is also consistent with data for other pathogens [43–45]. Figure 3 illustrates this relationship between antibody levels and protection graphically.

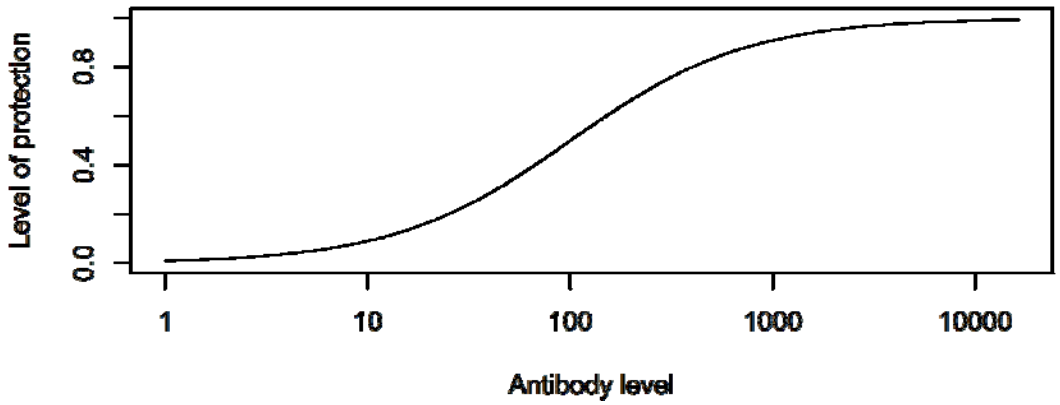

Figure 3 Protection as function of antibody levels ($k_1 = 1$, $k_2 = \log(100)$).

Our model represents antibodies in units of numbers of antibodies. In general, experimental studies report antibody neutralizing titers or similar assay-specific units. For this reason, and because we have no data for the correlation between antibody titers and protection for either the HPIV or IAV data we analyze, it is impossible to determine specific choices for and for our study systems. We instead chose values such that the antibody levels considered span the full range from low to high protection levels. Specifically, we set and where is the range of antibody levels predicted by our model for different inoculum doses and is the expected value. This choice is essentially arbitrary and therefore the protection curves we present below are to be understood conceptually.

Quantifying Morbidity

It is still not fully understood how virus and immune response affect host morbidity, i.e. the severity of symptoms. For virus infections, host morbidity can result in virus-induced death of infected cells, as well as immune response mediated pathology. A study of influenza infection in humans showed that a model in which symptom score was proportional to innate cytokine levels provided an adequate fit to the data [48]. Another study of influenza infections used a combination of innate cytokine (interferon) levels and cell death to define morbidity as , where is the total number of dead cells, and was chosen to be a sigmoidal mapping of log interferon levels [49]. Similarly, a previous model for dengue infections assumed that morbidity was proportional to the peak of the innate response, i.e. [50]. In the case of vaccines, strong pathological effects such as the death of a meaningful fraction of target cells do not occur. It therefore seems most reasonable to express morbidity (strength of symptoms) as a function of the innate immune response.

To obtain an estimate for a mapping between innate immune response and morbidity, we use data from a previously reported challenge experiment of influenza infection in human volunteers [28]. We use the reported values for different components of the local innate

response (IFN-a, IL6, IL8, and TNF-a) and, after scaling each component to a maximum value of 1, sum them to obtain an estimate for the total innate response strength. This total response quantity is again scaled and then mapped to morbidity, measured as total symptom score. Figure 4 shows the data.

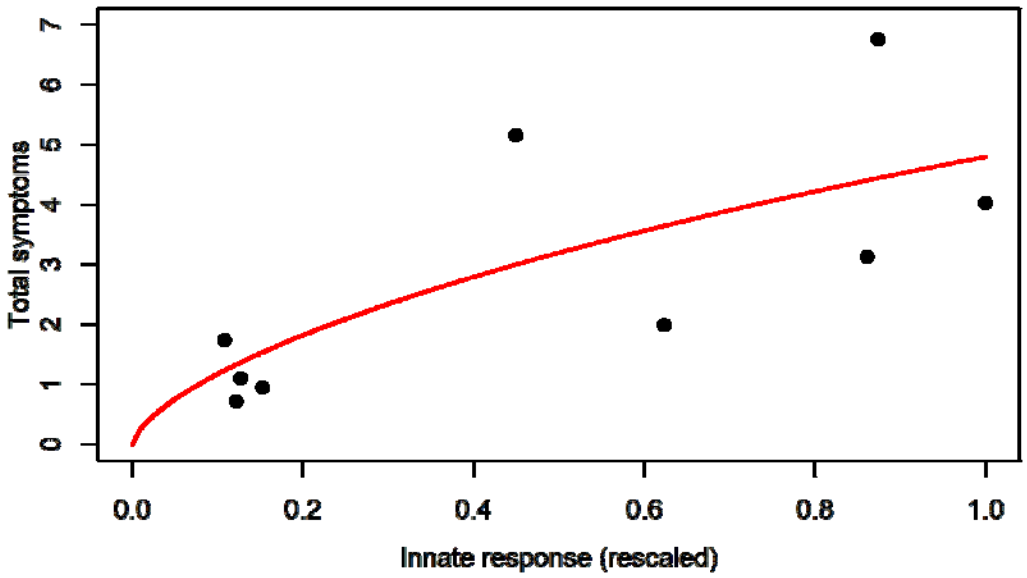

Figure 4 Data and best fit model for the connection between immune response and symptoms.

Also shown is the best fit of a sigmoidal model that provides a mapping between innate response and morbidity. The model is given by

---

where is morbidity as measured by total symptom score, and is the scaled innate response. Best fit parameter values are = 6.5 and = 0.66. The parameter was fixed at 36, corresponding to the maximum score possible based on the study protocol [28]. While a simpler linear model would fit the data equally well, it is less biologically reasonable since it would allow an unbounded increase in symptoms.

From our simulations, we obtain the time course of the innate response, . After rescaling this quantity, we use equation (3) to compute the time course for morbidity, . Finally, we take the integral of the morbidity over the duration of the infection to compute total morbidity as the area under the morbidity curve (MAUC). Since this approach mixes model simulations based on animal infections with morbidity estimates based on human data, the resulting morbidity curve should be interpreted in a similar conceptual way as the protection curve described above.

Immunity and pathogenesis as function of inoculum

After fitting the dynamical infection model (1) to each data set, we used the best-fit parameter values and ran simulations for a range of inoculum doses. Several time-series for the IAV and HPIV model simulations spanning the whole range of simulated inoculum doses are shown in figures 5 and 6.

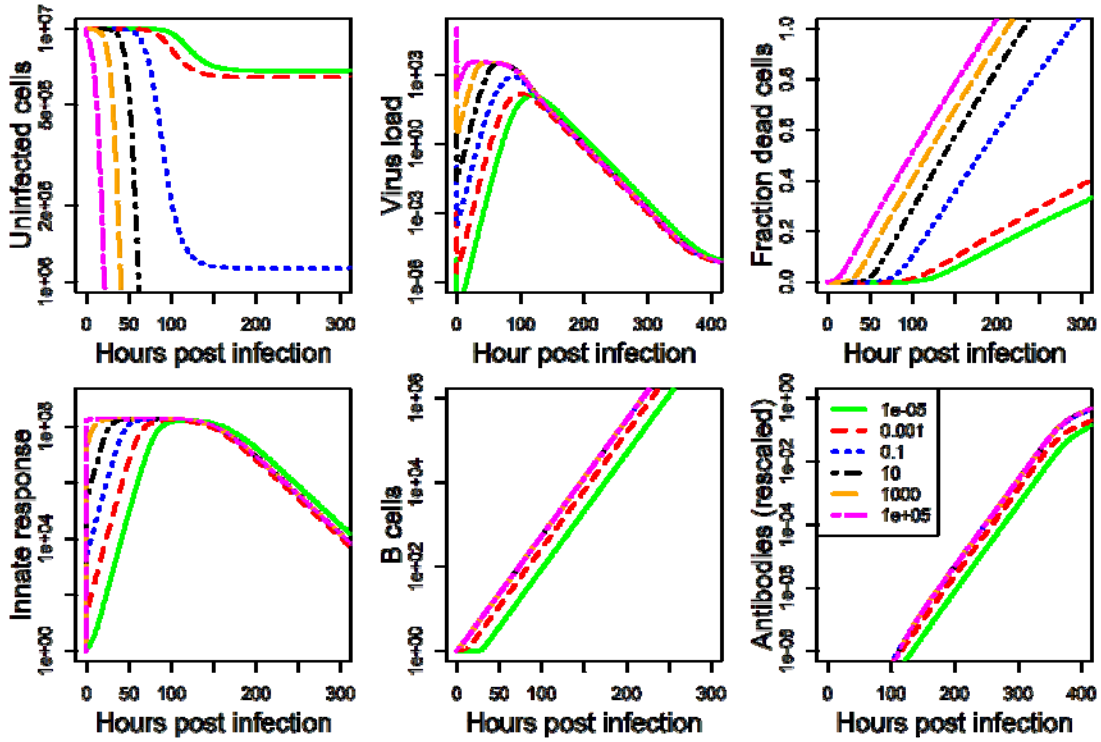

Figure 5 IAV model simulation for a range of inoculum doses.

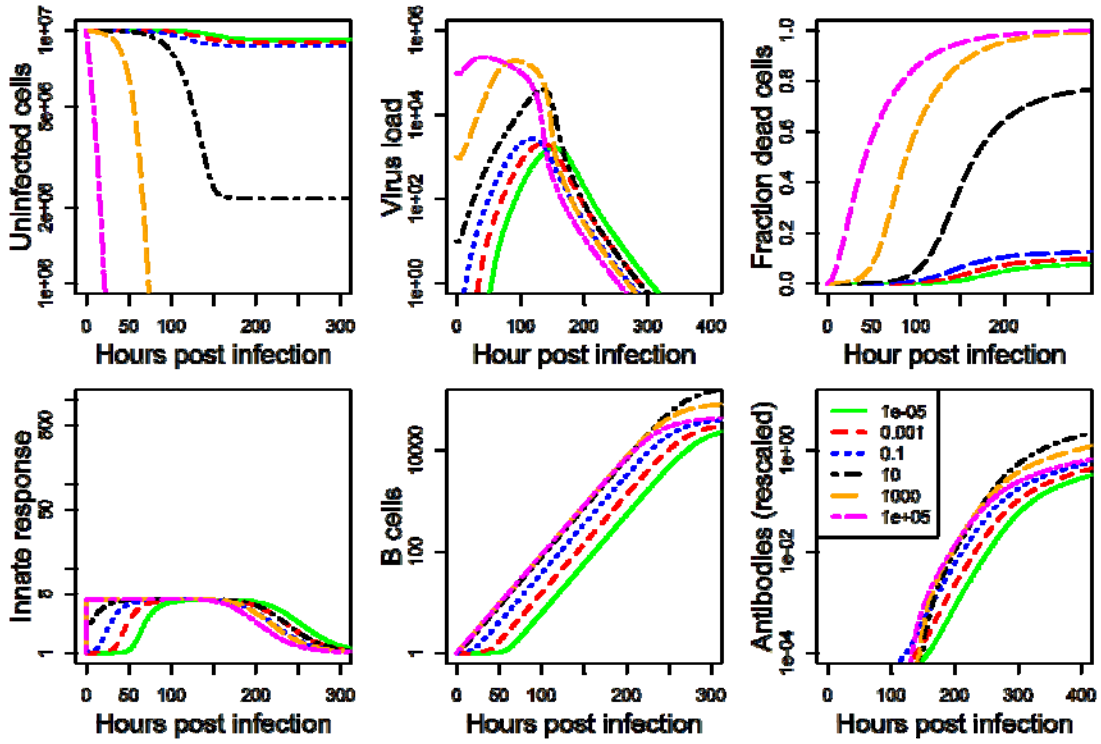

Figure 6 HPIV model simulation for a range of inoculum doses.

From these time-series, the level of protection and morbidity was computed. The model is simulated for 21 days, predicted antibodies are recorded at the final time. From these antibody levels, we compute immune protection using equation (2). We also record the predicted innate immune response, and, after scaling, use equation (3) to compute morbidity, and by integrating the area under the curve, determine the total amount of morbidity during the infection. Those results are shown for IAV are shown in figure 7, figure 8 shows results for HPIV.

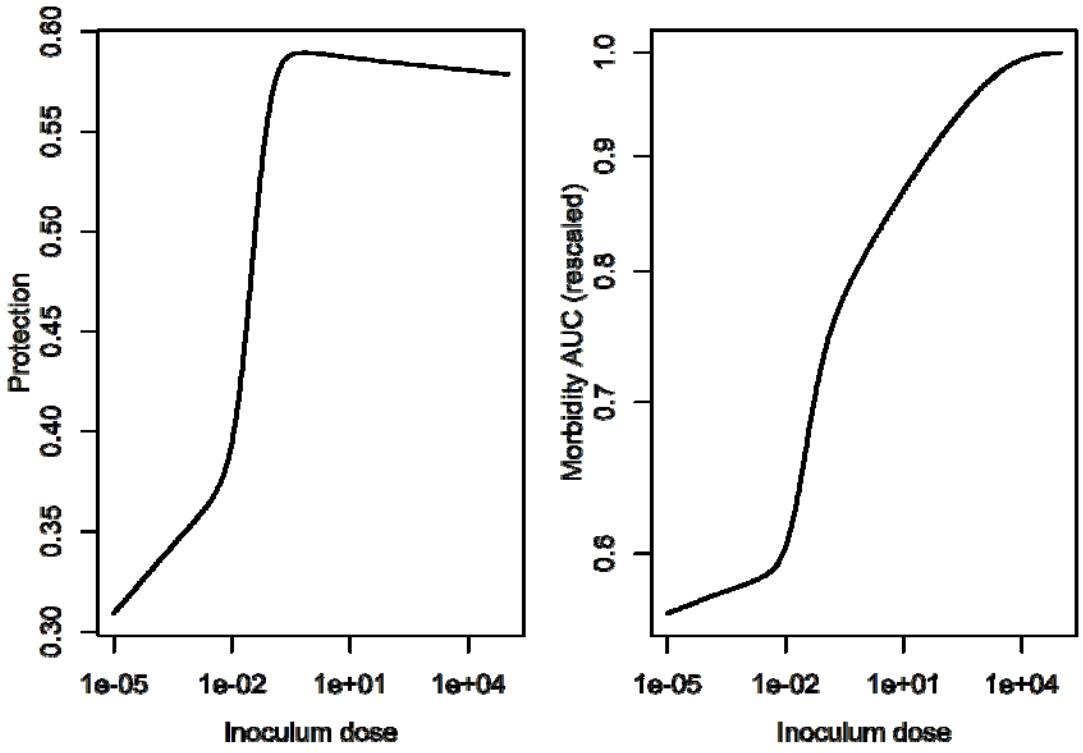

288

289 *Figure 7 Inoculum dependent protection and damage for the IAV infection model.*

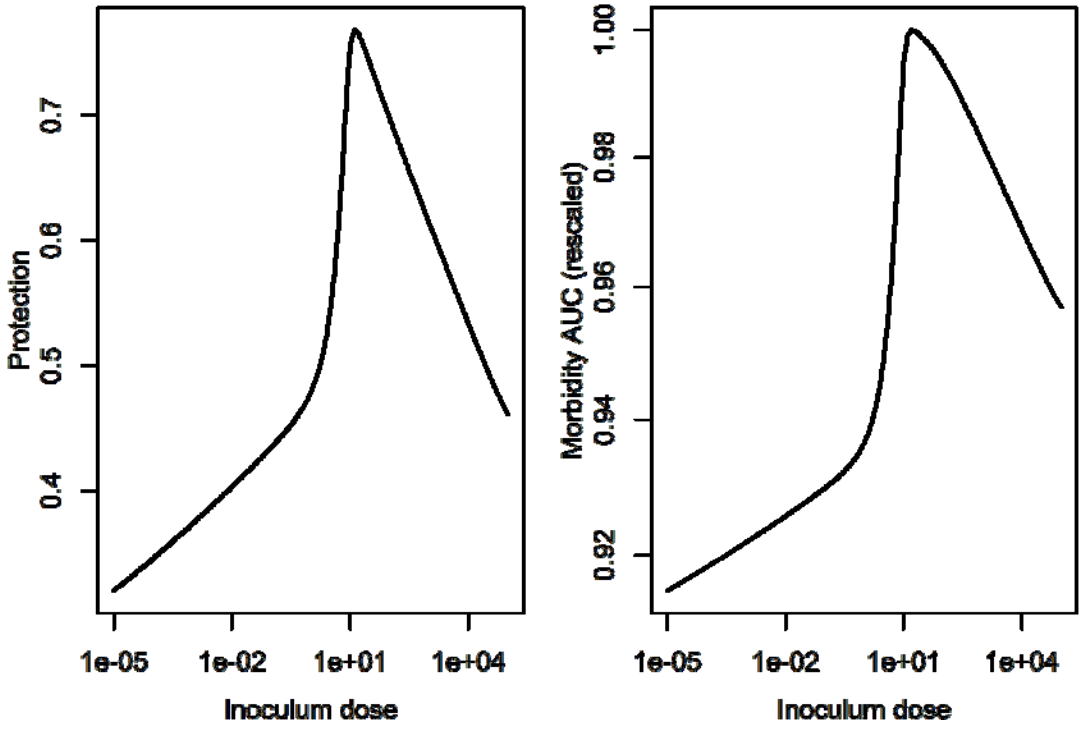

290

291 *Figure 8 Inoculum dependent protection and damage for the HPIV infection model.*

An inactivated vaccine model

The model and data above are for replicating pathogens, as such representing live, attenuated vaccines. Another important category of vaccines are those where the pathogen is killed and non-replicating. A modification of the above model can be used to simulate such a vaccine. For such a vaccine, cells do not get productively infected, and one can remove the variables tracking uninfected and infected cells. The model simplifies to

$$\begin{aligned} \text{Antigen} \quad \dot{P} &= -d_P P - k'_A A P \\ \text{Innate response} \quad \dot{F} &= p_F - d_F F + \frac{P}{P + h_V} g_F (F_{max} - F) \\ \text{B cells} \quad \dot{B} &= \frac{FP}{FP + h_F} g_B B \\ \text{Antibodies} \quad \dot{A} &= r_A B - d_A A - k_A A P \end{aligned}$$

We were not able to find data in the published literature for antigen (and possibly other model components) time series for different inoculum doses that would be detailed enough to allow model fitting. We therefore instead chose arbitrary values for model parameters that produced reasonable dynamics and explored the impact of inoculum/antigen dose on protection and morbidity for such a generic model. Figure 9 shows simulated time-series for different inoculum doses and figure 10 shows the resulting predicted immune protection and morbidity.

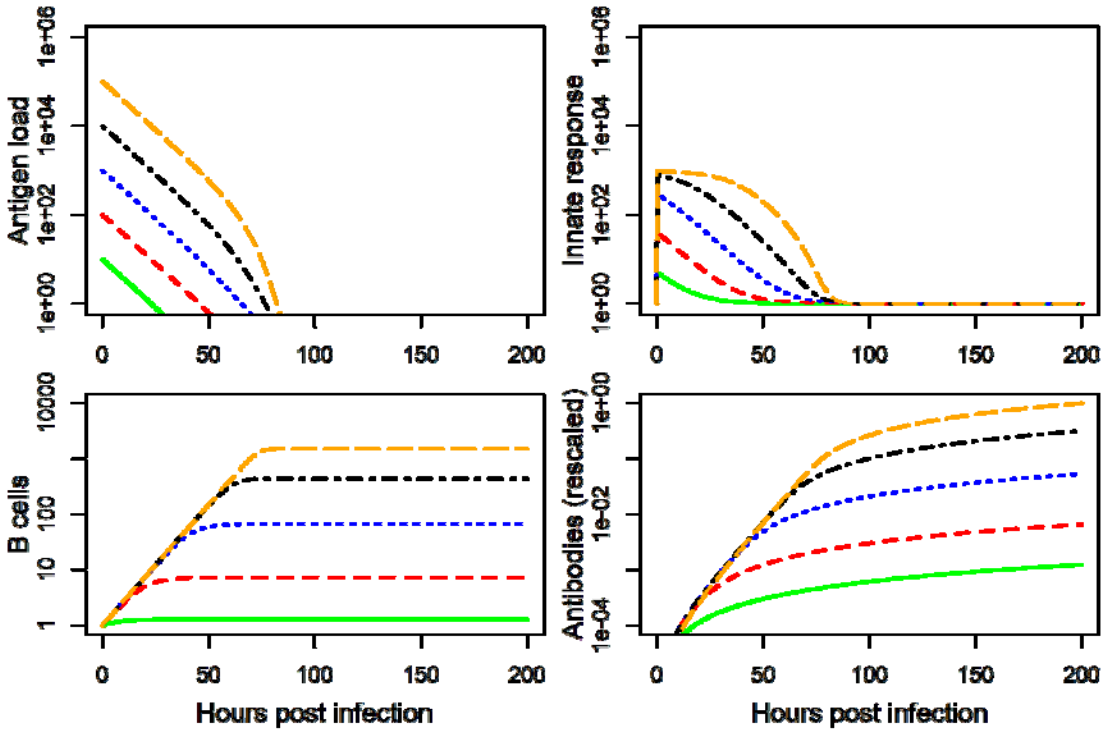

Figure 9 Model for non-replicating vaccine. Model parameters were set to , , , , , , , , . Initial conditions are F = 1, B = 1, A = 0 and varying values for antigen load.

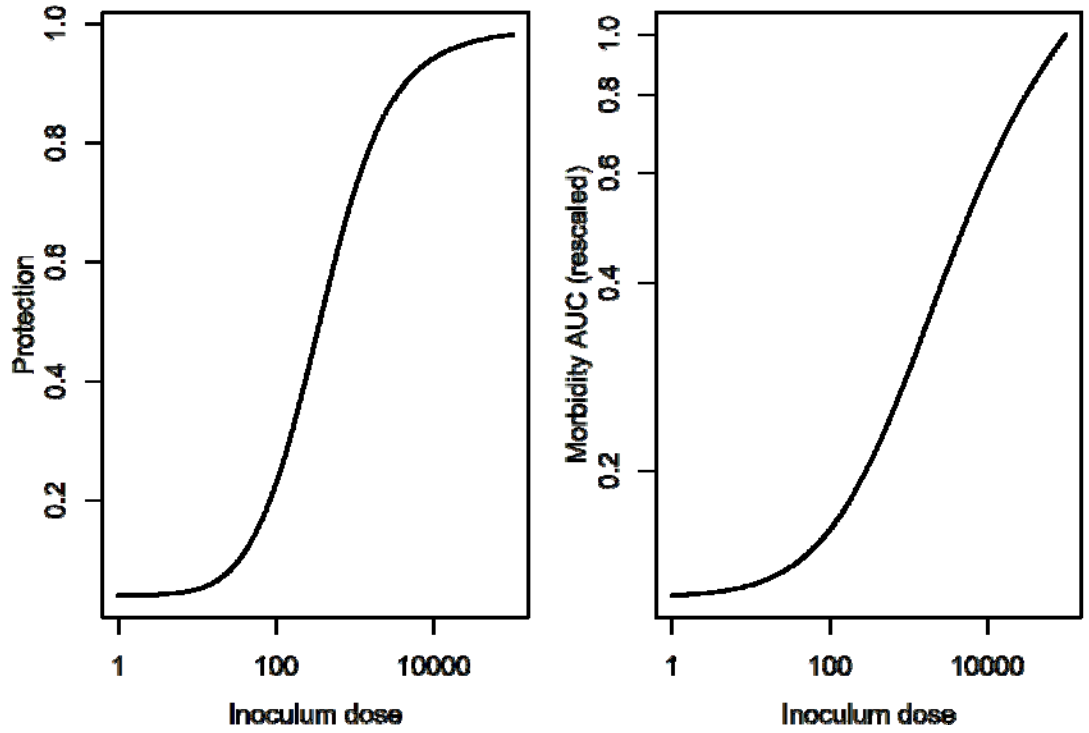

Figure 10 Inoculum dependent protection and damage for the inactivated vaccine model.

Optimal Inoculum dose illustration

Once immune protection and morbidity as a function of inoculum dose are predicted by the model, one can potentially determine optimal inoculum dose choices. The optimal amount depends on the main goals of the vaccine formulation. One could, for instance, choose a minimum acceptable level of immune protection or maximum acceptable level of morbidity, and determine the inoculum dose for those criteria. Another possibility is to compute and maximize a quantity that is a compound of immune protection and morbidity, with specific weights assigned to protection and morbidity. We illustrate this idea conceptually by looking at a very simple quantity, namely the ratio of immune protection to morbidity (as defined by the area under the curve), P/M. Figure 11 shows this quantity for the IAV and HPIV infections as well as for the inactivated vaccine.

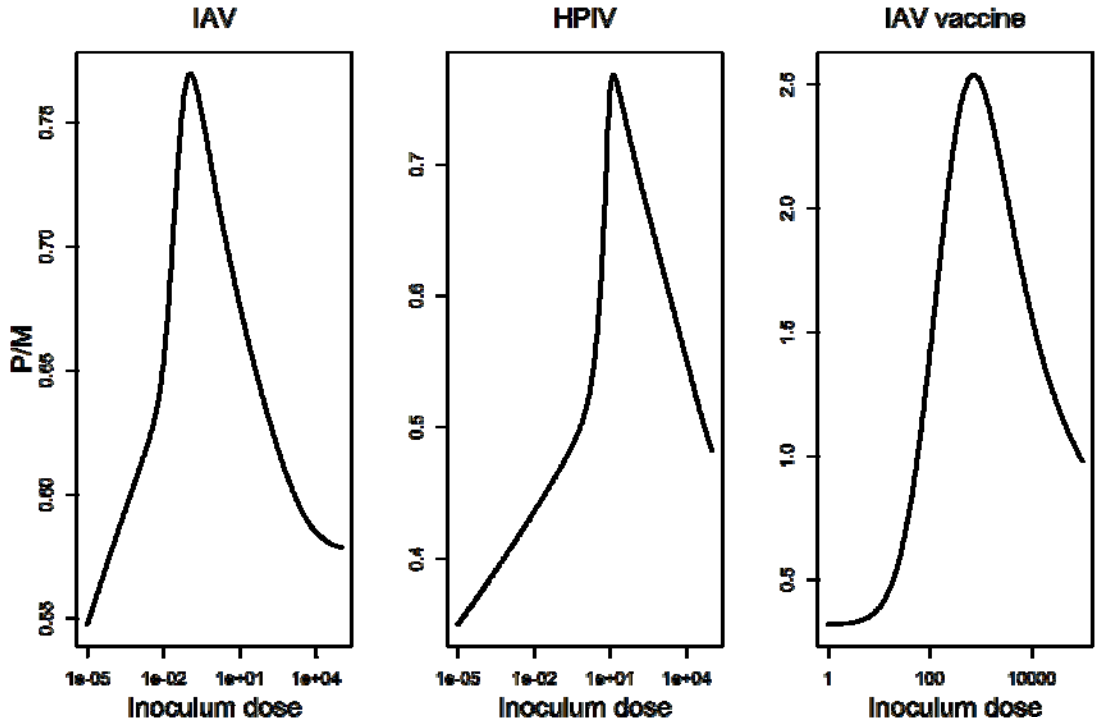

Figure 11 Ratio of protection, P, over morbidity, M, for different inoculum doses.

In each case, the amount of inoculum that leads to the highest ratio of P/MAUC occurs at an intermediate dose.

Discussion

In many situations, a higher inoculum dose of either live attenuated or killed antigen in a vaccine leads to a stronger immune response and subsequently likely better antibody or T-cell mediated immune protection [51]. However, this does not have to be universally true. Once inoculum doses increase beyond some threshold, the innate immune response might be triggered too strongly, which in turn could lead to an impaired adaptive immune

response and thus reduced immune protection. Similarly, while increased inoculum usually leads to more morbidity and stronger symptoms, this again might not be universal and depends on the interaction of pathogen and immune response.

In this study, we used a combination of data and models to explore how inoculum dose impacts immune protection and morbidity. We found that for the examples investigated, sometimes there is a monotonic or almost monotonic increase of protection and morbidity as inoculum increases (inactivated vaccine and IAV examples), while other times protection and morbidity can decline once dose increases beyond some value (HPIV example). For the illustrative example of an optimal dose based on a simple ratio of protection to morbidity, all our examples suggest that an intermediate amount of inoculum dose is optimal.

Our study fits into the recently proposed framework of Immunostimulation/Immunodynamic (IS/ID) modelling, which has been proposed as a framework to combine models and data for better vaccine formulation decisions [18], in analogy to the well-established pharmacokinetic/pharmacodynamic (PK/PD) modelling approach widely used in drug development [17].

We believe that using an approach that combines modeling with data can help in the development of more efficient vaccines. The key toward that goal is the availability and integration of the right kind of models and data. Since the data we analyzed is a mix of animal and human data and neither is complete enough to allow the whole modeling framework to be applied to it, the results presented here are to be considered mainly conceptually. The ideal type of data tracks antigen or pathogen load and different immune components over time, as well as morbidity (e.g. through weight loss in mice or symptom reports in humans) and includes immune protection data through challenge studies. Such data would need to be collected for several inoculum doses. Integrated with the models we analyzed here, it could then allow one to predict the impact over a full range of inoculum doses, including those not experimentally measured.

Being able to predict the expected protection achieved for a given inoculum dose can help in the design of vaccines in cases when only limited antigen is available, e.g. in emergency situations [4]. Having information on both immune protection and expected morbidity allows one to determine an optimal inoculum dose based on the - often conflicting - goals of high protection and low morbidity. For instance, one could systematically answer questions such as, “If we require at least 80% immune protection, what would the minimum amount of inoculum need to be? And what level of morbidity/side-effects would this induce?” Currently, both modeling and experiments are not yet able to be used in such a specific manner. However, a tighter integration of experiments with models, and further model refinement should allow one to use the modeling approach discussed here in the future to help design vaccines.

Some promising extensions and refinements of the models are inclusion of further components of the immune response. For instance, given that T-cells are also known to play an important role in immune protection and are affected by inoculum dose [52,53], it would be beneficial to extend experimental and modeling studies in the future and

consider both the B-cell and T-cell components of the adaptive response. Similarly, provided more detailed data on specific components of the innate response is available, including those components explicitly in the models might be useful. Another extension would be to consider stochastic models, which would better be able to capture variation among patients. This would require individual host data to be available for analysis and modeling.

To summarize, we developed a modeling framework that might allow a systematic and quantitative determination of the impact of different inoculum doses on resulting immune protection and morbidity. We applied this approach to several data sets to illustrate the general concept and show how it can lead to important insights, e.g. 'more inoculum does not always lead to more immune protection'. The modeling and analysis framework presented here can be applied to data from specific vaccine candidates and help to more efficiently determine the optimal dose.

Acknowledgements

We thank the Antia group members for helpful discussions.

AH, VZ and RA were partially supported by NIH/NIAID grant U19AI117891. KAP was partially supported by a NIH/NIGMS grant P20GM103499, SC INBRE. The funders had no role in study design, data collection and analysis, decision to publish, or preparation of the manuscript.

References

1. Ada G. Overview of vaccines and vaccination. Molecular biotechnology. 2005;29: 255–272. doi:10.1385/MB:29:3:255

2. Marois I, Cloutier A, Garneau É, Richter MV. Initial infectious dose dictates the innate, adaptive, and memory responses to influenza in the respiratory tract. Journal of leukocyte biology. 2012;92: 107–121. doi:10.1189/jlb.1011490

3. Falsey AR. Half-dose influenza vaccine: Stretching the supply or wasting it? Archives of internal medicine. 2008;168: 2402–2403. doi:10.1001/archinte.168.22.2402

4. Monath TP, Woodall JP, Gubler DJ, Yuill TM, Mackenzie JS, Martins RM, et al. Yellow fever vaccine supply: A possible solution. Lancet (London, England). 2016;387: 1599–1600. doi:10.1016/S0140-6736(16)30195-7

5. Crotty S, Ahmed R. Immunological memory in humans. Seminars in Immunology. 2004;16: 197–203. doi:10.1016/j.smim.2004.02.008

6. Seder RA. T-cell quality in memory and protection: Implications for vaccine design. Nature Reviews Immunology. 2008;8: 486.

7. R R. Bridging the knowledge gaps in vaccine design. Nature Biotechnology. 2007;25: 1361–1366.

8. Pulendran B, Ahmed R. Immunological mechanisms of vaccination. Nature Immunology. 2011;12: 509–517. doi:10.1038/ni.2039

9. Amanna IJ, Slifka MK. Wanted, dead or alive: New viral vaccines. Antiviral Research. 2009;84: 119–130. doi:10.1016/j.antiviral.2009.08.008

10. Bernstein DI, Falloon J, Yi T. A randomized, double-blind, placebo-controlled, phase 1/2a study of the safety and immunogenicity of a live, attenuated human parainfluenza virus type 3 vaccine in healthy infants. Vaccine. Cincinnati Children's Hospital Medical Center, University of Cincinnati, 3333 Burnet Avenue, Cincinnati, OH 45229, USA. david.bernstein@cchmc.org; 2011;29: 7042–7048. doi:10.1016/j.vaccine.2011.07.031

11. Karron RA, Thumar B, Schappell E, Surman S, Murphy BR, Collins PL, et al. Evaluation of two chimeric bovine-human parainfluenza virus type 3 vaccines in infants and young children. Vaccine. 2012;30: 3975–3981. doi:10.1016/j.vaccine.2011.12.022

12. Koopman G, Mooij P, Dekking L, Mortier D, Nieuwenhuis IG, Heteren M van, et al. Correlation between virus replication and antibody responses in macaques following infection with pandemic influenza a virus. Journal of virology. 2015;90: 1023–1033. doi:10.1128/JVI.02757-15

13. Treanor J, Keitel W, Belshe R, Campbell J, Schiff G, Zangwill K, et al. Evaluation of a single dose of half strength inactivated influenza vaccine in healthy adults. Vaccine. 2002;20: 1099–1105.

14. Cooper CL, Davis H, Cameron DW. Influenza vaccination with 1/10th the full dose. The New England journal of medicine. 2004;351: 2339–2340. doi:10.1056/NEJM200411253512219

15. Martins RM, Maia M de LS, Farias RHG, Camacho LAB, Freire MS, Galler R, et al. 17DD yellow fever vaccine: A double blind, randomized clinical trial of immunogenicity and safety on a dose-response study. Human vaccines & immunotherapeutics. 2013;9: 879–888. doi:10.4161/hv.22982

16. Campi-Azevedo AC, Almeida Estevam P de, Coelho-Dos-Reis JG, Peruhype-Magalhães V, Villela-Rezende G, Quaresma PF, et al. Subdoses of 17DD yellow fever vaccine elicit equivalent virological/immunological kinetics timeline. BMC infectious diseases. 2014;14: 391. doi:10.1186/1471-2334-14-391

17. Ambrose PG, Bhavnani SM, Rubino CM, Louie A, Gumbo T, Forrest A, et al. Pharmacokinetics-pharmacodynamics of antimicrobial therapy: It's not just for mice anymore. Clinical infectious diseases : an official publication of the Infectious Diseases Society of America. 2007;44: 79–86. doi:10.1086/510079

18. Rhodes SJ, Zelmer A, Knight GM, Prabowo SA, Stockdale L, Evans TG, et al. The tb vaccine h56+ic31 dose-response curve is peaked not saturating: Data generation for new

446 mathematical modelling methods to inform vaccine dose decisions. Vaccine. 2016;
447 doi:10.1016/j.vaccine.2016.10.060

448 19. Wong S-S, Webby RJ. Traditional and new influenza vaccines. Clinical microbiology
449 reviews. 2013;26: 476–492. doi:10.1128/CMR.00097-12

450 20. Reed G, Jewett PH, Thompson J, Tollefson S, Wright PF. Epidemiology and clinical
451 impact of parainfluenza virus infections in otherwise healthy infants and young children <5
452 years old. The Journal of Infectious Diseases. 1997;175: 807–813. Available:
453 http://www.jstor.org/stable/30129412

454 21. Hall CB. Respiratory syncytial virus and parainfluenza virus. The New England Journal
455 of Medicine. 2001;344: 1917–1928. Available: http://search.proquest.com.proxy-
456 remote.galib.uga.edu/docview/223949760?accountid=14537

457 22. Lee M-S, Walker RE, Mendelman PM. Medical burden of respiratory syncytial virus and
458 parainfluenza virus type 3 infection among US children: Implications for design of vaccine
459 trials. Human Vaccines. 2004;1: 5–11. doi:10.4161/hv.1.1.1424

460 23. Schmidt AC, Schaap-Nutt A, Bartlett EJ, Schomacker H, Boonyaratanakornkit J, Karron
461 RA, et al. Progress in the development of human parainfluenza virus vaccines. Expert
462 Review of Respiratory Medicine. 2011;5: 515–526. doi:10.1586/ERS.11.32

463 24. Schomacker H, Schaap-Nutt A, Collins PL, Schmidt AC. Pathogenesis of acute respiratory
464 illness caused by human parainfluenza viruses. Current Opinion in Virology. 2012;2: 294–
465 299. doi:10.1016/j.coviro.2012.02.001

466 25. Sato M, Wright PF. Current status of vaccines for parainfluenza virus infections.
467 [miscellaneous article]. Journal October 2008. 2008;27.
468 doi:10.1097/INF.0b013e318168b76f

469 26. GINSBERG HS, HORSFALL FL. Quantitative aspects of the multiplication of influenza a
470 virus in the mouse lung; relation between the degree of viral multiplication and the extent
471 of pneumonia. The Journal of experimental medicine. 1952;95: 135–145.

472 27. Ottolini MG, Porter DD, Hemming VG, Hensen SA, Sami IR, Prince GA. Semi-permissive
473 replication and functional aspects of the immune response in a cotton rat model of human
474 parainfluenza virus type 3 infection. J Gen Virol. 1996;77: 1739–1743. doi:10.1099/0022-
475 1317-77-8-1739

476 28. Hayden FG, Fritz R, Lobo MC, Alvord W, Strober W, Straus SE. Local and systemic
477 cytokine responses during experimental human influenza a virus infection. relation to
478 symptom formation and host defense. The Journal of clinical investigation. 1998;101: 643–
479 649. doi:10.1172/JCI1355

480 29. Li Y, Handel A. Modeling inoculum dose dependent patterns of acute virus infections.
481 Journal of theoretical biology. 2014;347: 63–73. doi:10.1016/j.jtbi.2014.01.008

30. Beauchemin CAA, Handel A. A review of mathematical models of influenza a infections within a host or cell culture: Lessons learned and challenges ahead RID g-4619-2011. Bmc Public Health. 2011;11. doi:10.1186/1471-2458-11-S1-S7

31. Smith AM, Perelson AS. Influenza a virus infection kinetics: Quantitative data and models. Wiley Interdisciplinary Reviews: Systems Biology and Medicine. 2011;3: 429–445. doi:10.1002/wsbm.129

32. Dobrovolny HM, Reddy MB, Kamal MA, Rayner CR, Beauchemin CAA. Assessing mathematical models of influenza infections using features of the immune response. PLoS ONE. 2013;8: e57088. doi:10.1371/journal.pone.0057088

33. Cao P, Yan AW, Heffernan JM, Petrie S, Moss RG, Carolan LA, et al. Innate immunity and the inter-exposure interval determine the dynamics of secondary influenza virus infection and explain observed viral hierarchies. PLoS computational biology. Public Library of Science; 2015;11: e1004334.

34. Pawelek KA, Huynh GT, Quinlivan M, Cullinane A, Rong L, Perelson AS. Modeling within-host dynamics of influenza virus infection including immune responses. PLoS Computational Biology. 2012;8: 1–13. doi:10.1371/journal.pcbi.1002588

35. Bartlett EJ, Hennessey M, Skiadopoulos MH, Schmidt AC, Collins PL, Murphy BR, et al. Role of interferon in the replication of human parainfluenza virus type 1 wild type and mutant viruses in human ciliated airway epithelium. Journal of virology. 2008;82: 8059–8070. doi:10.1128/JVI.02263-07

36. Potter CW, Oxford JS. Determinants of immunity to influenza infection in man. British medical bulletin. 1979;35: 69–75.

37. Handel A, Longini IM, Antia R. Towards a quantitative understanding of the Within-Host dynamics of influenza a infections. Journal of The Royal Society Interface. 2010;7: 35–47. doi:10.1098/rsif.2009.0067

38. Pawelek KA, Dor D, Salmeron C, Handel A. Within-host models of high and low pathogenic influenza virus infections: The role of macrophages. PloS one. 2016;11: e0150568. doi:10.1371/journal.pone.0150568

39. R Development Core Team. R: A language and environment for statistical computing [Internet]. Vienna, Austria: R Foundation for Statistical Computing; 2012. Available: http://www.R-project.org/

40. Johnson SG. The nlopt nonlinear-optimization package.

41. Soetaert K, Petzoldt T, Setzer RW. Solving differential equations in r: Package deSolve. Journal of Statistical Software. 2010;33: 1–25. doi:10.18637/jss.v033.i09

42. Mark Mitchell BM, al TW et. Engauge digitizer software [Internet]. Available: http://markummitchell.github.io/engauge-digitizer/

518 43. Qin L, Gilbert PB, Corey L, McElrath MJ, Self SG. A framework for assessing
519 immunological correlates of protection in vaccine trials. J Infect Dis. Statistical Center for
520 HIV/AIDS Research; Prevention, Fred Hutchinson Cancer Research Center, Seattle, WA,
521 USA. lqin@scharp.org; 2007;196: 1304–1312. doi:10.1086/522428

522 44. Plotkin SA. Vaccines: Correlates of vaccine-induced immunity. Clin Infect Dis. Sanofi
523 Pasteur, Doylestown, Pennsylvania, USA. stanley.plotkin@sanofipasteur.com; 2008;47:
524 401–409. doi:10.1086/589862

525 45. Gilbert PB, Qin L, Self SG. Evaluating a surrogate endpoint at three levels, with
526 application to vaccine development. Stat Med. Fred Hutchinson Cancer Research Center;
527 Department of Biostatistics, University of Washington, Seattle, WA 98109, USA.
528 pgilbert@scharp.org; 2008;27: 4758–4778. doi:10.1002/sim.3122

529 46. Coudeville L, Bailleux F, Riche B, Megas F, Andre P, Ecochard R. Relationship between
530 haemagglutination-inhibiting antibody titres and clinical protection against influenza:
531 Development and application of a bayesian random-effects model. BMC Med Res Methodol.
532 Sanofi pasteur, 2 avenue Pont Pasteur F-69367 Lyon cedex 07 France.
533 laurent.coudeville@sanofipasteur.com; 2010;10: 18. doi:10.1186/1471-2288-10-18

534 47. Feldstein LR, Matrajt L, Elizabeth Halloran M, Keitel WA, Longini IM Jr, H5N1 Vaccine
535 Working Group. Extrapolating theoretical efficacy of inactivated influenza a/h5n1 virus
536 vaccine from human immunogenicity studies. Vaccine. Center for Inference; Dynamics of
537 Infectious Diseases, Fred Hutchinson Cancer Research Center, Seattle, WA, United States;
538 Department of Biostatistics, College of Public Health; Health Professions; College of
539 Medicine, University of Florida, Gainesville, FL, United States. Electronic address:
540 ilongini@ufl.edu. 2016;34: 3796–3802.

541 48. Canini L, Carrat F. Population modeling of influenza A/H1N1 virus kinetics and
542 symptom dynamics. J Virol. 2011;85: 2764–2770. doi:10.1128/JVI.01318-10

543 49. Saenz RA, Quinlivan M, Elton D, MacRae S, Blunden AS, Mumford JA, et al. Dynamics of
544 influenza virus infection and pathology. Journal of Virology. 2010;84: 3974–3983.
545 doi:10.1128/JVI.02078-09

546 50. Ben-Shachar R, Koelle K. Minimal within-host dengue models highlight the specific roles
547 of the immune response in primary and secondary dengue infections. Journal of the Royal
548 Society, Interface. 2015;12. doi:10.1098/rsif.2014.0886

549 51. Akondy RS, Johnson PLF, Nakaya HI, Edupuganti S, Mulligan MJ, Lawson B, et al. Initial
550 viral load determines the magnitude of the human cd8 t cell response to yellow fever
551 vaccination. Proceedings of the National Academy of Sciences of the United States of
552 America. 2015;112: 3050–3055. doi:10.1073/pnas.1500475112

553 52. Estcourt MJ, Létourneau S, McMichael AJ, Hanke T. Vaccine route, dose and type of
554 delivery vector determine patterns of primary cd8+ t cell responses. European journal of
555 immunology. 2005;35: 2532–2540. doi:10.1002/eji.200535184

53. Wang Z, Kedzierski L, Nuessing S, Chua BYL, Quiñones-Parra SM, Huber VC, et al. Establishment of memory cd8+ t cells with live attenuated influenza virus across different vaccination doses. The Journal of general virology. 2016;97: 3205–3214. doi:10.1099/jgv.0.000651